# Applications of a general random-walk theory for confined diffusion

Elisa M. Calvo-Muñoz,[1] Myvizhi Esai Selvan,[1] Ruichang Xiong,[1] Madhusudan Ojha,[2] David J. Keffer,[1,*] Donald M. Nicholson,[3] and Takeshi Egami[2,4]

[1]*Department of Chemical and Biomolecular Engineering, University of Tennessee, Knoxville, Tennessee 37996, USA*

[2]*Department of Physics and Astronomy, University of Tennessee, Knoxville, Tennessee 37996, USA*

[3]*Computer Science and Mathematics Division, Oak Ridge National Laboratory, Oak Ridge, Tennessee 37831, USA*

[4]*Materials Science and Technology Division, Oak Ridge National Laboratory, Oak Ridge, Tennessee 37831, USA*

(Received 2 September 2010; published 24 January 2011)

A general random walk theory for diffusion in the presence of nanoscale confinement is developed and applied. The random-walk theory contains two parameters describing confinement: a cage size and a cage-to-cage hopping probability. The theory captures the correct nonlinear dependence of the mean square displacement (MSD) on observation time for intermediate times. Because of its simplicity, the theory also requires modest computational requirements and is thus able to simulate systems with very low diffusivities for sufficiently long time to reach the infinite-time-limit regime where the Einstein relation can be used to extract the self-diffusivity. The theory is applied to three practical cases in which the degree of order in confinement varies. The three systems include diffusion of (i) polyatomic molecules in metal organic frameworks, (ii) water in proton exchange membranes, and (iii) liquid and glassy iron. For all three cases, the comparison between theory and the results of molecular dynamics (MD) simulations indicates that the theory can describe the observed diffusion behavior with a small fraction of the computational expense. The confined-random-walk theory fit to the MSDs of very short MD simulations is capable of accurately reproducing the MSDs of much longer MD simulations. Furthermore, the values of the parameter for cage size correspond to the physical dimensions of the systems and the cage-to-cage hopping probability corresponds to the activation barrier for diffusion, indicating that the two parameters in the theory are not simply fitted values but correspond to real properties of the physical system.

DOI: 10.1103/PhysRevE.83.011120 PACS number(s): 05.40.Fb, 68.43.Jk, 83.10.Rs

## I. INTRODUCTION

Atomic and molecular diffusion is a fundamental transport process in fluids. In recent years, the transport of chemical species through nanoscale pores, tubes and channels has become very important in many areas [1] and an increasing number of materials with such configurations are being produced and applied. [2] As a result, there has been an increase in experimental and theoretical interest to investigate diffusion processes in nanoscale confined geometries. [3,4] Confinement restricts and complicates molecular motion. Molecular diffusion in bulk fluids follows the Einstein relation, [5] in which the mean square displacement (MSD), a single-particle autocorrelation function, is linearly proportional to observation time, in the infinite-time limit. It has been shown that in macroscopic pores, this conventional diffusion is maintained. [6] Taken to an extreme, confinement can result in MSDs which do not obey the Einstein relation, such as those exhibited in one-dimensional hard-rod theory [7] or in small cylindrical pores in which particle passing is not observed. [4,8] Even in confined systems that obey Einstein's relation, there are physical phenomena that arise due to confinement, such as percolation, [9] in which irregular confinement blocks some paths for transport, resulting in a reduction of the diffusion coefficient. In this regime of three-dimensional systems with nanoscale confinement, there is the particular challenge of relating the observed diffusivity to the structure of the material. To date, investigations of this structure-property relationship are performed on a case-by-case basis. It is the intention of this work to demonstrate that a straightforward incorporation of confinement into random-walk theory is capable of quantitatively describing diffusion in systems with nanoscale confinement, across a broad range of disparate materials.

Molecular-level simulation is an ideal tool for developing a fundamental molecular-level understanding of structure-property relationships. The advantage of molecular simulation lies in the fact that one has complete access to every trajectory of every atom at every instant in time, which can be analyzed in a broad variety of ways to gain insight into the system. Molecular dynamics (MD) simulations are routinely used to study diffusion in systems with nanoscale confinement, such as adsorbates in nanoporous adsorbents like zeolites and metal organic frameworks, [10] gases in polymeric membranes, [11] ions in solid conductors, [12] and many other applications. The primary drawback of (MD) simulation is that one is limited to systems that are small relative to macroscopic systems (typically on the order of $10^6$ or fewer atoms) and for short durations (typically on the order of 10 ns or less). Thus, diffusion phenomena that occur on larger length or time scales remain outside the domain of MD simulations.

Integrated multiscale modeling algorithms allow one to describe the physics of transport across a range of time scales using multiple techniques, in which the spatial and/or temporal resolution varies. For example, in one of the applications described below, the MD simulation of a hydrated proton exchange membrane [13] (PEM) employs a time step of 0.1 fs ($10^{-16}$ s) in order to capture the vibration of chemical bonds in the system. However, the MD simulations extend only for

*dkeffer@utk.edu

 

2 ns, which is insufficient to reach the infinite-time limit of the Einstein relation from which self-diffusivities can be extracted. For the same system, confined-random-walk (CRW) simulations fitted to the short-time MD results generate MSDs out to 100 ns ($10^{-7}$ s), which does reach the Einstein limit. Thus we cover nine orders of magnitude in time with an integrated multiscale modeling algorithm that combines MD and CRW simulations.

Random-walk (RW) theory and simulation have been used routinely to model diffusion processes. The simple isotropic random-walk model (SRW) is, indeed, the basis of most of the diffusive processes. A large body of work has accumulated concerning the properties of such processes, and very detailed information is available. [14,15] The traditional SRW considers that movements are uncorrelated and unbiased, that is, the location after each step taken in the random walk is only dependent on the location in the previous step, the process is Markovian with regard to the location, [16] and the direction moved in at each step is completely random. Assuming that movement in any direction is allowed, this process is essentially Brownian motion and such models produce the standard diffusion equation. However, as mentioned before, some systems show anomalous dynamical behavior, especially in short and intermediate observation times. Through numerous approaches (fractional Brownian motion, [17] generalized diffusion equations, [18] Langevin equations, [19] generalized Langevin equations, [20] generalized master equations, [21] generalized thermostatistics, [22] fractional equations [23]), the extension of random-walk theory has created a very rich tool, rich enough to be able to describe certain dynamic features of complex systems. Regarding diffusion in confined geometries, continuous-time random-walk models provide explanations for a variety of physical phenomena. Montroll and Shlesinger [24] give a good review of the general theory of random walks. Random walks have also been modified by simply introducing repelling, reflecting, or absorbing barriers. [25] Nevertheless, to the best of our knowledge, a simple theory of confined diffusion applicable to a large number of different materials that does not entail high computational expenses has not been reported.

In this work, we develop a theory of confined diffusion that describes the general features observed in the dynamics of atoms and/or molecules diffusing through materials with nanoscale confinement using the fewest number of parameters necessary to capture the essential physics. We begin with the conventional random-walk theory for systems without confinement, which depends only on the variance of the Maxwell-Boltzmann distribution, and then add two parameters that capture confinement: a cage size and a cage-to-cage hopping probability. As discussed below, the CRW theory and simulation generate three regimes of behavior in the short, intermediate, and long time scales. Because of its simplicity, the theory has modest computational requirements and is thus able to simulate systems with very low diffusivities for a sufficiently long time to reach the infinite-time regime where the MSD is linearly proportional to the observation time.

The MD-CRW approach is applied to three practical cases in which the degree of order in confinement varies. The three systems include diffusion of (i) polyatomic molecules in metal organic frameworks (MOFs), (ii) water in proton exchange membranes, and (iii) liquid and glassy iron. In the first system, the MOF is a rigid, crystalline adsorbent, in which the porous network is completely regular. In the second system, there is a nanoscale aqueous domain that interpenetrates the hydrophobic polymer phase. The aqueous domain through which water diffusion occurs is composed of irregularly shaped and irregularly connected water clusters. In the third system, glassy iron, there is no second component; each iron atom finds itself within a transient cage composed of neighboring iron atoms. The purpose in studying three systems is twofold. First, it demonstrates the broad applicability of the MD-CRW simulation approach. Second, it underscores the common physics governing confined diffusion in each of these three disparate systems. For all three cases, the CRW simulations are parametrized based on the short-time MSD of the MD simulations and are capable of quantitatively describing all of the observed short-time behavior. Furthermore, the CRW simulations are run for a sufficiently long time to generate MSDs in the linear regime, from which the self-diffusivity can be reliably regressed, with a small fraction of the computational expense associated with MD simulations.

## II. THEORY

The intent of the theory of confined diffusion developed and applied herein is to describe the general features observed in the dynamics of atoms and/or molecules diffusing through materials with nanoscale confinement using the fewest number of parameters necessary to capture the essential physics. To this end, we begin with the conventional random-walk theory for systems without confinement and then add two parameters that capture confinement. For systems without confinement, a three-dimensional Gaussian random walk is described by a series of steps in which a direction for each particle is chosen randomly and the velocities are sampled from the Maxwell-Boltzmann (MB) distribution. [14,26] For the unconfined system, there is only one independent parameter and it is the variance of the MB distribution. It is important that diffusing particles do not interact; each individual random walk is independent of all others. From an analysis of the mean square displacement, an averaged single-particle autocorrelation function can be defined as

$$X_{\mathrm{MSD}(\tau)} = \langle |\mathbf{r}_i(t+\tau) - \mathbf{r}_i(t)|^2 \rangle, \tag{1}$$

where $\mathbf{r}_i(t)$is the position of particle $i$ at time $t$ and $\tau$ is an observation or elapsed time. The angled brackets indicate an average over both particles $i$ and time $t$. The Einstein relation relates the self-diffusion coefficient of the particles to the MSD in the infinite-time limit,

$$D = \frac{1}{2d} \lim_{\tau \to \infty} \frac{X_{\mathrm{MSD}}}{\tau}, \tag{2}$$

where $d$ is the dimensionality of the system.

In a RW simulation, a single step has an average displacement $\Delta r$, and each step has a time associated with it, $\Delta t$. These parameters are related to the temperature through the first and second moments of the MB distribution with variance $\sigma_v^2$,

$$\sigma_v^2 = \frac{k_B T}{m}, \tag{3}$$

$$\langle v \rangle = \frac{\langle \Delta r \rangle}{\Delta t} = \sqrt{\frac{8 k_B T}{\pi m}}, \tag{4}$$

$$\langle v^2 \rangle = \left\langle \left( \frac{\langle \Delta r \rangle}{\Delta t} \right)^2 \right\rangle = \frac{3 k_B T}{m}, \tag{5}$$

where $k_B$ is the Boltzmann constant, $T$ is the temperature, $m$ is the mass of the diffusing particle, and $\langle v \rangle$ is the mean speed. Thus, in a RW simulation one can generate the MSD as a function of $\tau$ and obtain the self-diffusivity in Eq. (2), specifying only the MB distribution. Furthermore, the diffusivity from an unconfined three-dimensional (3D) RW simulation is given by

$$D_0 = \frac{\sigma_v^2 \Delta t}{2}. \tag{6}$$

This expression provides a limiting value of the diffusivity in the absence of confinement and is hereafter referred to as the intrinsic diffusivity of the unconfined system. As a note, in an unconfined system, the RW theory is not capable of reproducing the very short-time ballistic motion of particles, in which the MSD is proportional to $\tau^2$, because the ballistic regime is limited to time scales before the first collision and the RW theory models Brownian motion that occurs after many collisions.

Confinement is incorporated in the RW theory through the addition of two parameters: a cage size $R_{\text{cage}}$ and a cage-to-cage hopping probability $p_{\text{cage}}$. In our confined-random-walk theory, the particles themselves have no volume and originate at the center of a cage, which is assumed to be spherical. Each particle engages in a conventional random walk until its displacement from its original position is greater than $R_{\text{cage}}$. At the end of a step in which a particle has stepped beyond a cage, that move is accepted with probability $p_{\text{cage}}$. If the move was unsuccessful, the particle is reflected back into the original cage, such that the net length of its trajectory is maintained. If the move is successful, the particle now resides in a new spherical cage with a center located at a distance $R_{\text{cage}}$ from the edge of the original cage and lying along a vector collinear with the particle's trajectory. The successful and unsuccessful cage-to-cage moves are shown schematically in Fig. 1. As clearly indicated in the schematic of a successful move, overlap of the new cage and the old cage will always occur except when the trajectory of the particle is perfectly parallel to the local radial vector.

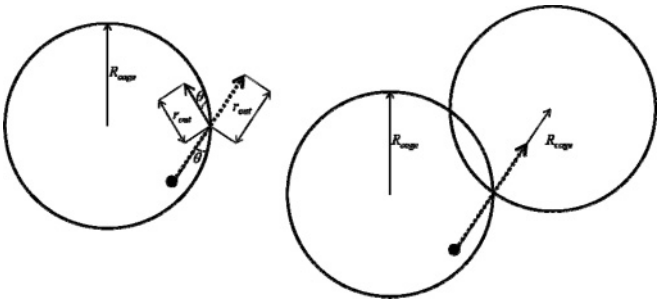

FIG. 1. Schematic of unsuccessful and successful cage-to-cage moves. On the left, an unsuccessful move is reflected back into the original cage, maintaining the length of the trajectory. On the right, a successful move puts the particle in a new cage with center located a distance $R_{\text{cage}}$ along the vector of the trajectory.

Once a successful cage-to-cage move occurs, the particle is only aware of the position of the center of the current cage.

The placement of the new cage was chosen to ensure that any cage-to-cage move results in the particle always residing within the confines of the new cage. While the trajectory of the particle is pointed toward the center of the new cage after a successful cage-to-cage move, in the next step the direction of the move is once again randomly selected, which mitigates any bias introduced by this choice of new cage position.

While this model is extraordinarily simple, it is capable of reproducing a range of behavior from completely confined to completely unconfined diffusion. It yields intermediate behavior due to confinement and infinite-time diffusivities, if run for a sufficiently long time. Furthermore, we show below that after being parametrized to the short-time MSDs obtained from MD simulations, it is capable of quantitatively capturing the intermediate- and long-time dynamic behavior of three diverse applications, in which the degree of order in confinement varies. The three systems include diffusion of (i) polyatomic molecules in metal organic frameworks, (ii) water in proton exchange membranes, and (iii) liquid and glassy iron.

## III. SIMULATION METHODS

### A. Confined-random-walk simulations

The confined random walk simulations were implemented in a serial code written in FORTRAN90. The variance of the Maxwell-Boltzmann distribution, the time scaling constant $\Delta t$, the cage size $R_{\text{cage}}$, and a cage-to-cage hopping probability $p_{\text{cage}}$ were provided as inputs. Two hundred particles were simulated to demonstrate the general capabilities of the theory (Figs. 4 and 5) and 1000 particles were simulated when parametrizing the model in the three applications. The number of steps used in the simulations varied from $10^4$ to $10^7$ and depended strongly on the parameters input into the simulation. The goal was to simulate sufficiently long to reach the infinite-time limit required by the Einstein relation, so that self-diffusivities could be obtained from Eq. (2). As $p_{\text{cage}}$ decreased, the time required to reach this limit increased. The MSDs were generated after the simulation was completed from a file containing positions of the particles at periodic intervals. In all simulations, at least 1000 points along the trajectory were saved. From simulations one could only obtain statistically reliable MSDs of about half of the time of the simulation, before the diminishing amount of data in the correlation function rendered the rest of the MSD unacceptably noisy [27]. Therefore we calculated the self-diffusivity coefficients in a range of observation times running from $t_{\text{sim}}/4$ to $t_{\text{sim}}/2$, where $t_{sim}$ is the simulation duration. The nonzero lower limit was needed to omit information prior to the infinite-time limit.

### B. Molecular dynamics simulations

The CRW theory is compared to three systems, for which MSDs are available from MD simulations. The first system is of an explosive, RDX (hexahydro-1,3,5-trinitro-1,3,5-triazine, CAS no. 121-82-4), adsorbed in an isoreticular metal organic framework, IRMOF-1. The structures of RDX and IRMOF-1 are shown in Fig. 2. [28] The cages are cubic in shape with

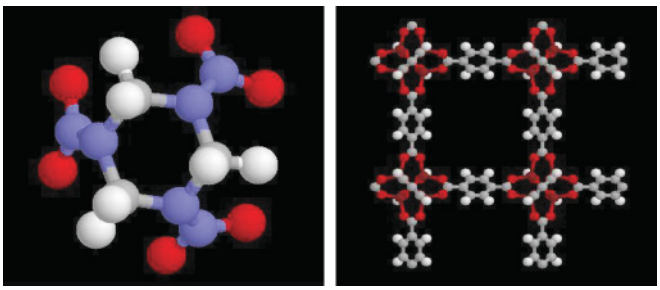

FIG. 2. (Color online) Structures of RDX (on the left) and IRMOF-1 (on the right). Color legend: blue, N; red, O; gray, C; white, H; maroon, Zn.

octahedral zinc-carboxylate complexes at the vertices and benzene rings along the edges. The dimension of the cage is 12.92 Å. IRMOF-1 has been synthesized and characterized. [29] Xiong *et al.* have previously simulated RDX in IRMOF-1, [30] IRMOF-10, [31] and other IRMOFs. [32] Similar dynamic behavior of RDX is observed for all IRMOFs and for the purposes of this demonstration, we use the results from IRMOF-1 [32]. The simulations were performed across a temperature range from 300 to 600 K, in order to obtain an activation energy for cage-to-cage diffusion.

A complete discussion of the interaction potential and simulation method is given in the Ref. [30]. Here we provide a brief summary. For RDX, we employ a nonreactive, fully flexible, atomistic interaction potential for RDX that takes features from both Wallis and Thompson as well as Boyd *et al.* [33] The RDX intramolecular force field includes bond stretching, angle bending, torsion, and nonbonded interactions. The nonbonded interactions include Lennard-Jones interactions and Coulombic interactions, due to a permanent charge distribution, modeled as point charges at each atom center. It has been pointed out that there is a significant variation in the charge distribution of IRMOF-1 depending on the quantum mechanical calculation method applied [34]. Herein we have used the results obtained using the Löwdin population analysis (LPA) method [35]. The atoms of IRMOF-1 are fixed at their crystallographic coordinates and interact with the RDX through Lennard-Jones (LJ) and Coulombic interactions, with parameters from Tafipolsky *et al.*, [36] in which the LJ parameters are taken from Allinger *et al.*, [37] which is the same source for LJ parameters used for RDX.

Classical equilibrium MD simulations were performed on an in-house parallel code written in FORTRAN90 to obtain configurations and diffusivities of RDX adsorbed in IRMOF-1. We integrated the equations of motion using the two-time-step reversible REference System Propagation Algorithm (r-RESPA) of Tuckerman and co-workers. [38] Intramolecular degrees of freedom were accounted for in the short-time loop, with a step size of 0.2 fs. There were ten short steps per long time step. The temperature was controlled using the Nosé-Hoover thermostat [39]. We equilibrated the system for 2 ns. Following equilibration, we simulated an additional 8 ns for data collection. During data production, positions of the center of mass of the RDX molecules were saved every 5 ps and were used to calculate the self-diffusivity via the Einstein relation. Uncertainties in the self-diffusivity are reported as the standard deviations of the $x$, $y$, and $z$ components of the diffusivity.

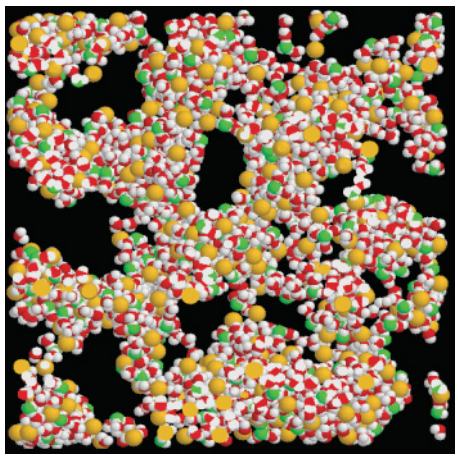

FIG. 3. (Color online) Cross section from a snapshot of a molecular dynamics simulation of Nafion (EW = 1144) at 300 K and a water content of $\lambda = 6$. In this snapshot, all atoms except the sulfur of Nafion have been rendered invisible. Color legend: white, H; red, O of water; green, O of hydronium ion; orange, S.

The second system simulated is the hydrated proton exchange membrane Nafion. We have previously reported diffusion coefficients for water in PEMs as a function of side chain length, molecular weight, and equivalent weight (EW) of the polymer [13,40]. Across polymers, the same qualitative behavior of water dynamics is observed. In this work, we therefore, examine the diffusion coefficients of water in Nafion with an EW of 1144 and a degree of polymerization of 15. The structure of the hydrated Nafion 1144 is shown in Fig. 3. [28] In this figure, all atoms of Nafion have been rendered invisible except the sulfur of the sulfonate group, in order to better visualize the shape of the aqueous domain. Additional interactive structures and images are available for viewing and download on an archived site [28]. The diffusion coefficient of water in Nafion varies strongly with water content. Herein, we examine water contents ranging from minimally hydrated to saturated, $\lambda = 3, 6, 9, 15$, and 22 $H_2O/SO_3H$.

Here again we provide a brief summary of the MD simulation method and potentials used to generate the MSDs employed in this work. The potential model for Nafion was taken from the literature. It is an explicit atom model with the exception of the $CF_X$ groups, which are treated as united atoms. The potential includes bond stretching, bond bending, and bond torsion modes. It also includes nonbonded interactions using the Lennard-Jones potential and a Coulombic interaction. The details of the potential model have been published in previous studies by other authors. [41,42] Water is simulated using the TIP3P model [43] with a flexible OH bond. [42] The model for hydronium ions, $H_3O^+$, is from Urata *et al.* [44] Classical equilibrium MD simulations of hydrated Nafion were performed on an in-house parallel code written in FORTRAN90. The integrator, thermostat, and technique for capturing diffusivities are analogous to what was done in the MD simulations of RDX in IRMOFs.

The third system we compare to is liquid and glassy iron. We use the Johnson potential for interactions [45]. Because these simulations were much less computationally intensive than those required for the previous two applications, we

used a simpler in-house MD serial code with the single-time-step fifth-order gear-predictor corrector as an integrator [46]. The thermostat was the same. The glassy configuration was generated by taking an equilibrium configuration of liquid iron at 3000 K and instantly quenching it to 300 K. After an equilibration period, the MSD were recorded and analyzed according to the procedure described above. In contrast to the previous two applications, these MSDs are not previously published. In addition, the CRW theory was also applied to liquid iron at 3000 K.

## IV. RESULTS

We organize the results into four sections. In the first section, we provide a description of the range of capabilities of the confined-random-walk theory. In the subsequent three sections, we apply it to each of the three test systems.

### A. General predictions of the confined-random-walk Theory

Before applying the confined-random-walk theory to the three applications, we first present a brief demonstration of the capabilities of the theory. The purpose of this section is not only to show that two parameters, a cage size and a cage-to-cage hopping probability, are indeed capable of capturing the dynamic behavior from fully confined to fully unconfined systems, but also to clearly illustrate the effect that changing either parameter has on the system behavior. An understanding of the parametric sensitivity of the model in a generic sense will aid in the interpretation of the results when the theory is applied to the three target systems.

In Fig. 4, we plot the MSD as a function of observation time on linear and logarithmic scales for a dimensionless system in which $\langle \Delta r \rangle = 2.87 \times 10^{-3}$, $\Delta t = 1$, $R_{\text{cage}} = 1$, and the probability of a successful cage-to-cage hop, $p_{\text{cage}}$, was varied from 0 to 1. When $p_{\text{cage}} = 0$, the particles are completely confined within their original cage. When $p_{\text{cage}} = 1$, all cage-to-cage hops were successful and we recovered the unconfined RW theory, regardless of the value of $R_{\text{cage}}$. All of these simulations were carried out to the infinite-time limit, in which the MSD was linearly proportional to the observation time. The CRW theory is able to reproduce the spectrum of behaviors within the two asymptotes mentioned above. The expected linear proportionality between the MSD and the observation time, which is characteristic of a system without confinement, is seen when $p_{\text{cage}} = 1$. This is clearly indicated by the corresponding straight line with a slope of unity in the log-log plot. For the completely confined system ($p_{\text{cage}} = 0$) no hop was successful. The MSD displays an initial period of linear behavior, which is due to diffusion within the cage before the particle interacts with the walls. As particles do not diffuse beyond the cage, the self-diffusion coefficient in the infinite-time-limit region must be, and was indeed found to be, zero. Intermediate behavior was detected when $0 < p_{\text{cage}} < 1$. Because of confinement, the MSD vs observation time curves are not linear at intermediate times. As can be seen in the linear plots, the long-time slopes (proportional to the self-diffusivity) decrease as $p_{\text{cage}}$ decreases, which is in agreement with the fact that confinement slows diffusion. All systems reach the infinite-time-limit regime if run long enough, as can be seen in the log-log plot from the common slope of unity of for all curves with nonzero $p_{\text{cage}}$. The time required to reach this limit, however, varies depending on the $p_{\text{cage}}$ value. Systems with very low diffusivities (systems with small cage-to-cage probability) reach the infinite-time limit more slowly. This dramatic slowing of the diffusion is the primary reason that computationally intensive techniques such as molecular dynamics simulations may not alone be able to generate self-diffusivities in highly confined systems.

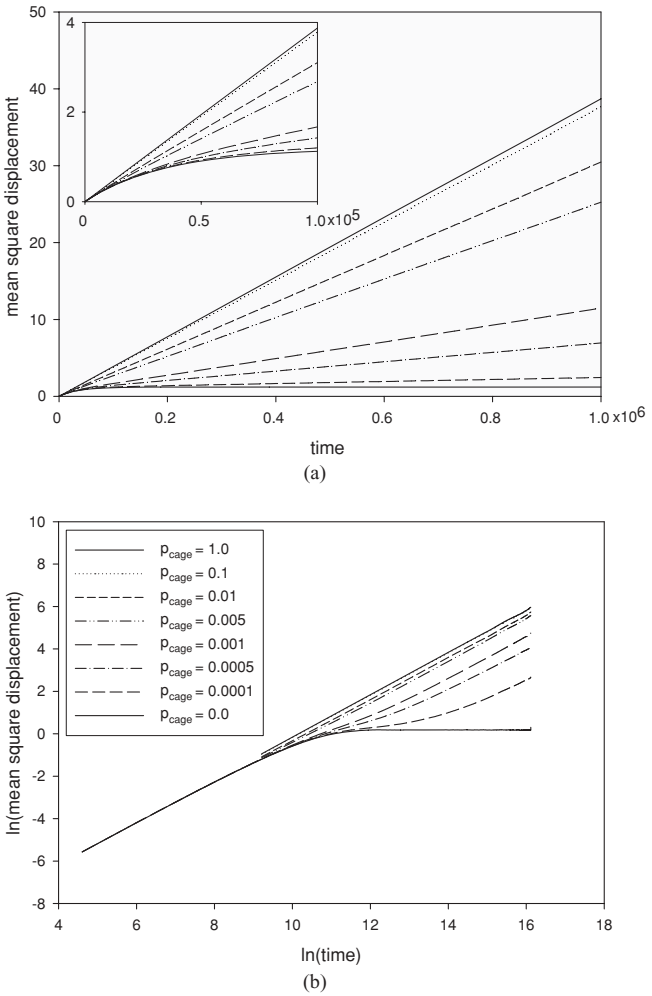


FIG. 4. Impact of cage-to-cage hopping probability $p_{\text{cage}}$. Plot of the mean square displacement as a function of observation time on linear (a) and logarithmic (b) scales for a dimensionless system in which $\langle \Delta r \rangle = 2.87 \times 10^{-3}$, $\Delta t = 1$, $R_{\text{cage}} = 1$, and $p_{\text{cage}}$ is varied from 0 to 1.

Figure 4(b) illustrates that there are three time regimes for the MSD for systems with nonzero $p_{\text{cage}}$. At the shortest times, there is a regime in which the confinement has not yet been felt and the linear behavior is observed with a slope corresponding to the intrinsic diffusivity of the unconfined system. The second regime is the intermediate-time regime, in which confinement is influencing the MSD and the relationship between the MSD and the observation time is sublinear. The third regime is the infinite-time limit, in which the MSD is once again linear with observation time, now with a slope that corresponds to the effective diffusivity of the confined system.

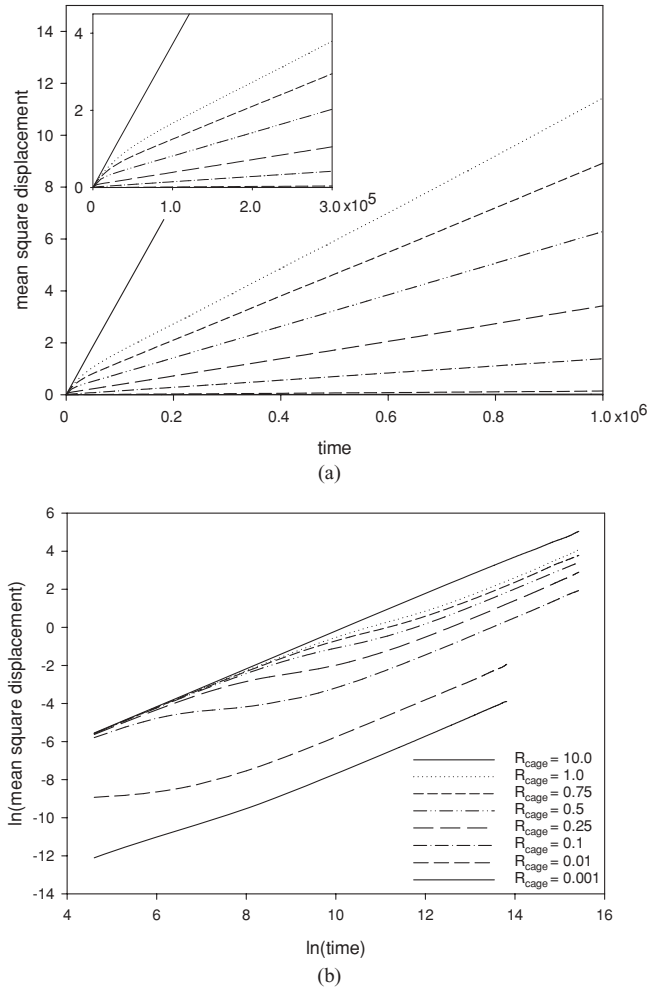


FIG. 5. Impact of cage radius $R_{\text{cage}}$. Plot of the mean square displacement as a function of observation time on linear (a) and logarithmic (b) scales for a dimensionless system in which $\langle \Delta r \rangle = 2.87 \times 10^{-3}$, $\Delta t = 1$, $p_{\text{cage}} = 0.001$, and $R_{\text{cage}}$ is varied from 0 to 10.

In Fig. 5, we plot the MSD as a function of observation time on linear and logarithmic scales for a dimensionless system in which $\langle \Delta r \rangle = 2.87 \times 10^{-3}$, $\Delta t = 1$, $p_{\text{cage}} = 0.001$, and the size of the cage, $R_{\text{cage}}$, is varied from 0 to 10. In the limit that $R_{\text{cage}}$ approaches infinity, we recover the unconfined RW theory, regardless of the value of $p_{\text{cage}}$. We observe that a decrease in the cage size causes a decrease in the self-diffusivity, again in agreement with the general idea that confinement slows diffusion.

Figure 5(b) also demonstrates that all MSDs exhibit three regimes. What can be observed particularly clearly in Fig. 5(b) is the fact that the duration of the short-time regime (linear behavior with unconfined diffusivity) is governed by the cage size. In Fig. 5, for a cage size of 10.0, only the short-time regime is visible. As the cage size decreases, the duration of this regime shrinks. In the inset of the linear plot, Fig. 5(a), one can also see that the general point where the curve "bends over" increases as the case size increases.

Having examined the impact of $p_{\text{cage}}$ and $R_{\text{cage}}$, we can also study the impact of temperature on self-diffusion. A change in temperature changes the variance of the MB distribution and also changes the intrinsic diffusivity of the unconfined system, Eq. (6). For many confined systems, diffusion is surface mediated and there is an activation barrier associated with a cage-to-cage move. Thus the diffusivity obeys an Arrhenius temperature dependence,

$$D = D_0 \exp\left(-\frac{E_a}{k_B T}\right). \tag{7}$$

Typically, the cage-to-cage hopping probability contains the activation barrier,

$$p_{\text{cage}} = c \exp\left(-\frac{E_a}{k_B T}\right), \tag{8}$$

where $c$ is a normalization constant. Thus a change in $p_{\text{cage}}$ could be caused by a change in activation energy (e.g., a different material) or a change in temperature in the same material.

### B. Application to diffusion of polyatomic molecules in metal organic frameworks

The CRW theory was applied in the first place to diffusion of an explosive, RDX, adsorbed in an isoreticular metal organic framework, IRMOF-1. This system provides a standard by which the capabilities of the more coarse-grained CRW theory can be tested. It is a standard because the MSDs can be generated out to the infinite-time limit via MD simulation. [30] Thus we have reliable self-diffusion coefficients from a more finely resolved technique. Furthermore, the porous network is rigid and uniform, with well-defined cubic cages with a length of 12.92 Å. [29] Thus we can judge whether the size parameter $R_{\text{cage}}$ correctly captures the real size of the confinement. Furthermore, the MD simulations have been performed over a range of temperatures, yielding an activation energy for diffusion of 6.0 kcal/mol. Thus, we can judge whether the cage-to-cage hop probability captures the activated energy of the diffusivity, as assumed in Eq. (8).

For each one of the seven available sets of MSD data (corresponding to temperatures of 300, 350, 400, 450, 500, 550, and 600 K) the CRW theory was applied. We adjusted $p_{\text{cage}}$, $R_{\text{cage}}$, and $\Delta t$ in order to obtain a first approximate fit to the MSD data from the MD simulations. Then, we refined this set of parameters in a subsequent optimization procedure using the Limited memory Broyden-Fletcher-Goldfarb-Shanno method for Bounded problems (L-BFGS-B) method, [47] which performs a nonlinear multivariate optimization on bounded variables. In our case, the three variables are bounded: $0 < p_{\text{cage}} < 1$, $0 < R_{\text{cage}}$, and $0 < \Delta t$.

Figure 6 shows a comparison between the mean square displacement from MD simulations and the mean square displacement obtained with the CRW model for the seven different temperatures. With the appropriate parametrization, the agreement between CRW and the MD results is excellent. The CRW theory is capable of reproducing the diffusive behavior of RDX in IRMOF-1 in all the studied range of temperatures. The numerical values of the parameters and the diffusivities from the MD and CRW simulations are given in Table I. The average error between the MD and CRW self-diffusivities is 1.7%. Uncertainties in the self-diffusivity are reported as the standard deviations of the $x$, $y$, and

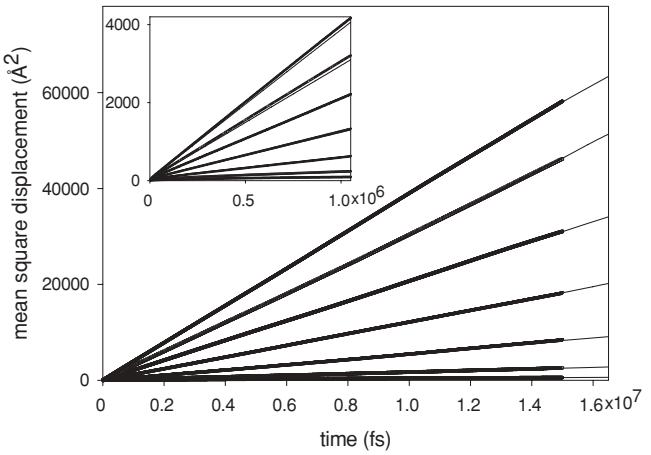


FIG. 6. Comparison of the mean square displacement from MD (symbols) and CRW simulation (lines) for diffusion of RDX in IRMOF-1 at different temperatures. From the bottom to the top: 300, 350, 400, 450, 500, 550, and 600 K.

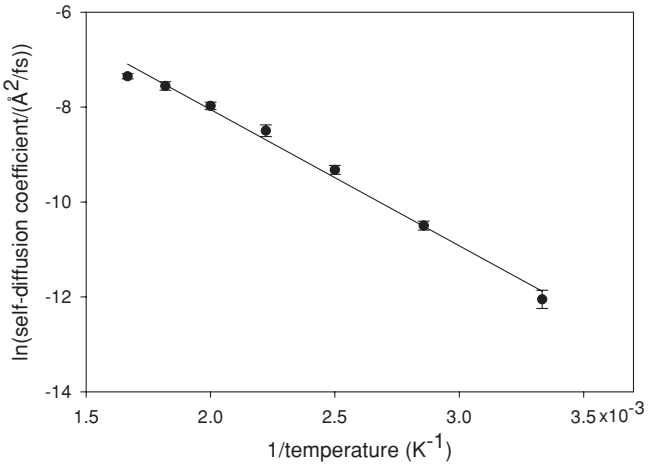


FIG. 7. Arrhenius plot showing the diffusivities (obtained from the CRW model) for the RDX–IRMOF-1 system as a function of temperature.

$z$ components of the diffusivity. In Table I, we observe that $R_{\text{cage}}$ is approximately constant with an average of 8.46 Å. In our attempt to develop the simplest possible theory, all the cages in the model are assumed to be spherical. IRMOF-1 does not exhibit spherical cages but cubic ones with a length of 12.92 Å. A sphere that encloses the same volume as a cube of 12.92 Å has a radius of 8.01 Å. Therefore, it appears that $R_{\text{cage}}$, the parameter that represents the dimension of the confinement space in our theory, shows good agreement with the size of the physical cage in the material.

In constrast to $R_{\text{cage}}$, both $p_{\text{cage}}$ and $D_0$ depend on the temperature, as they should via Eqs. (6) and (8), respectively. There is a qualitative similarity between the MSDs for RDX in IRMOF-1 (Fig. 6) and the MSDs for the generic system in which $p_{\text{cage}}$ is varied [Fig. 4(a)], because changing the temperature in the physical system changes the cage-to-cage hopping probability, as hopping from cage to cage is an activated process with an Arrhenius temperature dependence. In Fig. 7, we plot the CRW self-diffusivity as a function of temperature in an Arrhenius plot. We find an activation energy for diffusion of 5.7 kcal/mol, as compared to the value of 6.0 kcal/mol reported by Xiong *et al.* [30] from the MD simulations. This temperature dependence predominantly lies in the cage-to-cage hop probability. The temperature dependence of $D_0$ is more complicated than what Eq. (6) would predict and is a consequence of activated motion between multiple adsorption sites within each cage, a feature present in the MD simulations but omitted from the more coarsely grained CRW level of description.

### C. Application to diffusion of water in proton exchange membranes

The CRW theory was also applied to the diffusion of water in the PEM Nafion (EW = 1144) at 300 K as a function of water content. It has previously been reported that the diffusion coefficient of water in Nafion varies strongly with water content from both experiment [48] and simulation [13]. Thus, herein we examine different water contents including from minimally hydrated to saturated, $\lambda = 3$, 6, 9, 15, and 22 $H_2O/SO_3H$. This system is considerably different from the one presented above, as it does not present well-defined physical cages, but amorphous water clusters whose size and connectivity vary depending on the water content.

For each one of the studied systems, we had mean square displacement data available from two different molecular dynamics simulations. The first set of simulations was only run for short observation times (no longer than 0.37 ns), while in the second set, MSDs from 0.5 to 1 ns were collected [13]. The infinite-time limit was not reached in any case, due to computational limitations. In the longer MD simulations, the

TABLE I. Properties of the MD and CRW simulations applied to the diffusion of RDX in IRMOF-1 as a function of temperature. In this case, the MD simulations were run to the long-time limit and should agree with the diffusivity of the CRW simulations.

| | CRW theory | | | | MD simulations |
|---|---|---|---|---|---|
| $T$ (K) | $D_0$ ($10^{-8}$) (m$^2$/s) | $R_{\text{cage}}$ (Å) | $p_{\text{cage}}$ | $D$ ($10^{-9}$) (m$^2$/s) | $D$ ($10^{-9}$) (m$^2$/s) |
| 300 | 0.037 | 8.10 | $1.20 \times 10^{-3}$ | $0.06 \pm 0.01$ | $0.056 \pm 0.005$ |
| 350 | 0.12 | 8.50 | $5.40 \times 10^{-3}$ | $0.28 \pm 0.03$ | $0.276 \pm 0.006$ |
| 400 | 0.35 | 8.07 | $1.89 \times 10^{-2}$ | $0.89 \pm 0.08$ | $0.94 \pm 0.03$ |
| 450 | 0.61 | 8.60 | $3.72 \times 10^{-2}$ | $2.0 \pm 0.3$ | $2.0 \pm 0.1$ |
| 500 | 0.91 | 9.35 | $6.00 \times 10^{-2}$ | $3.4 \pm 0.3$ | $3.5 \pm 0.3$ |
| 550 | 1.35 | 8.60 | $8.20 \times 10^{-2}$ | $5.2 \pm 0.5$ | $5.12 \pm 0.08$ |
| 600 | 1.94 | 8.03 | $1.04 \times 10^{-1}$ | $6.4 \pm 0.4$ | $6.5 \pm 0.2$ |

TABLE II. Properties of the MD and CRW simulations applied to the diffusion of water in Nafion as a function of water content. In this case, the MD simulations were not run to the long-time limit.

| | CRW theory | | | | MD simulations |
|---|---|---|---|---|---|
| $\lambda$ | $D_0$ ($10^{-9}$) ($m^2/s$) | $R_{cage}$ (Å) | $p_{cage}$ | $D$ ($10^{-9}$) ($m^2/s$) | $D$ ($10^{-9}$) ($m^2/s$) |
| 3 | 0.32 | 2.7 | $8 \times 10^{-4}$ | $0.044 \pm 0.003$ | $0.041 \pm 0.007$ |
| 6 | 0.910 | 6.9 | $3 \times 10^{-3}$ | $0.31 \pm 0.01$ | $0.26 \pm 0.05$ |
| 9 | 1.75 | 12.5 | $3 \times 10^{-3}$ | $0.64 \pm 0.01$ | $0.58 \pm 0.06$ |
| 15 | 2.66 | 17.5 | $6 \times 10^{-3}$ | $1.3 \pm 0.1$ | $1.2 \pm 0.2$ |
| 22 | 3.24 | 22.5 | $7 \times 10^{-3}$ | $1.73 \pm 0.07$ | $1.7 \pm 0.2$ |

exponent $X_{MSD} \propto \tau^m$ fell in a subdiffusive range of 0.6 to 0.8. In this application, we fitted the CRW theory only to the short-time simulations. Thus, the comparison of the CRW theory and the MSDs in the range from 0.5 to 1 ns is a prediction and explicitly not a fit.

The CRW parameters and the self-diffusivities of water from CRW and MD simulations are reported in Table II. Note that the MD simulations did not reach the long-time limit and there is some error associated with these self-diffusivities due to this shortcoming. From Fig. 8, we see immediately that we are able to model the short-time MSDs from MD very well. The CRW simulations thus parametrized yield MSDs in the 0.5 to 1 ns time range in excellent agreement with the longer MD simulations. Furthermore, the CRW simulations are carried out for much longer times, up to 100 ns, where the linear long-time behavior is reached. We note in Table II that there is not a great difference between the self-diffusivities extracted from the linear behavior of the CRW simulations and from the sublinear regime of the longer MD simulations. Regardless, there is a great deal of additional confidence in the CRW diffusivities now that it has been shown that they have been obtained in a limit rigorously corresponding to the Einstein relation.

There is great interest in characterizing the size and connectivity of the aqueous domain in PEMs. Various models have been proposed to describe this network [49]. Here, the CRW theory provides a characteristic dimension of the aqueous cluster size based on a dynamic property, the self-diffusivity of water, $R_{cage}$. The cage size increases with increasing water content, which is completely reasonable on a physical basis. Fourier transform of the water-water pair correlation function in hydrated Nafion generates characteristic periodicity with a characteristic dimension of 20–30 Å for $\lambda = 3$ to 6, [13] which includes the dimension of both the hydrophobic and hydrophilic phases. Whether the volume of these cages corresponds quantitatively to average volumes of water clusters in the PEM, as was the case for diffusion in the MOFs, is a subject requiring further analysis of the morphology of the aqueous domain from experiment and simulation. However, at this point, it remains a promising possibility. The CRW simulations also provide a probability of cage-to-cage hopping as a function of water content. Again, we believe that this may provide a crucial piece of evidence in understanding the fundamental mechanisms for the dependency of water diffusion in PEMs. Further analysis, while not the subject of this paper, is under way.

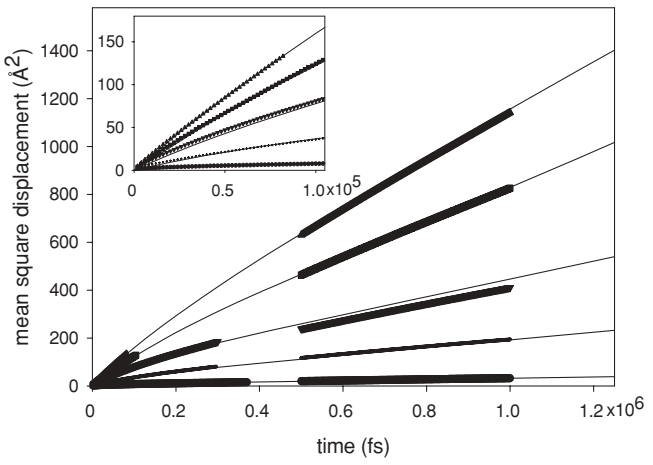


FIG. 8. Comparison of the mean square displacement from MD (symbols) and CRW simulation (lines) for diffusion of water in Nafion 1144 with different levels of hydration. From the bottom to the top $\lambda = 3$, 6, 9, 15, and 22 $H_2O/SO_3H$.

Throughout this work, we have attempted to minimize the number of parameters used in the CRW theory. Fixing the pore shape to spherical and having a single pore size resulted in one parameter to characterize pore size. Were we to allow a distribution of pore sizes and shapes, we would require additional parameters. Since we were able to capture the dynamic behavior of water in Nafion—a system where there clearly is a distribution of pore sizes and pore shapes in the real material—with a single-parameter model, we felt there was no justification for the needless introduction of additional parameters. That a single size parameter can describe the MSD behavior in this application also indicates that capturing the polydispersity in the pore size and shape is not a critical element in understanding and modeling the system.

### D. Application to the diffusion of liquid and glassy iron

Finally, we applied the CRW model to diffusion of liquid iron at 3000 K and glassy iron at 300 K. In contrast to the previous two applications, these MSDs are not previously published. The MSD from MD and CRW simulations at 300 K are shown in Fig. 9. The CRW parameters and the self-diffusivities of Fe from CRW and MD simulations are reported in Table III. The MSDs for the MD and CRW simulations at 3000 K are linear and consequently are not shown. There is no evidence of confinement present in liquid iron at 3000 K. However, the glassy iron does show significant confinement.

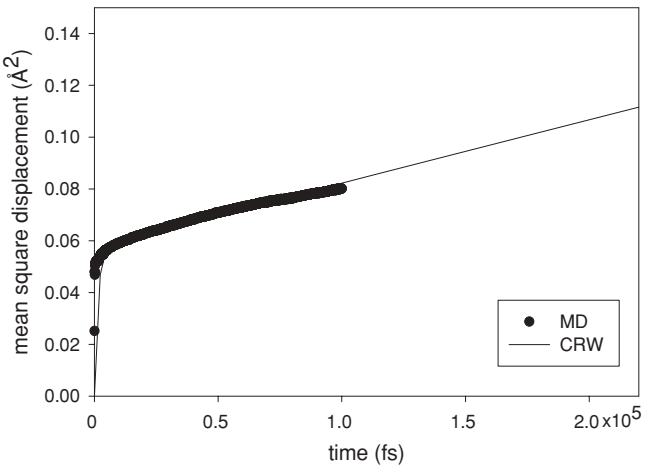


FIG. 9. Comparison of the mean square displacement from MD (symbols) and CRW simulation (lines) for diffusion of glassy iron at 300 K.

Dense random packing of hard spheres is commonly used as first-order structural models. [50] of glassy metals. Atoms vibrate within a cage of tightly packed neighbors and only certain circumstances generate a momentary change in the structure that allows some of them to move and diffuse. A collective molecular rearrangement (a chain reaction flow event) occurs due to thermal fluctuations [51]. The diffusivities of these systems are typically very small, which severely hinders obtaining the self-diffusivity coefficients using MD simulations. Analyses of the MSDs by simulations and by various theories yield a family of curves qualitatively similar to those shown in Fig. 4(b), where the variation of $p_{\text{cage}}$ has been replaced directly with temperature [52].

We note that the MSDs from MD simulation end at 0.1 ns. In order to reach the linear regime, the CRW simulations were run for 18 ns, where the slope of the double logarithmic plot of the MSD vs observation time was $0.95 \pm 0.02$. In this long-time regime, a value of $(4.0 \pm 0.1) \times 10^{-13}$ m$^2$/s was obtained for the self-diffusivity coefficient of Fe in the glassy state at 300 K. It is worth noting that MD simulations describe a glass formed by an instantaneous quench and are too short to capture key relaxation processes in the glass; therefore, the glass structure within which we calculate the MSD is not fully relaxed. This leads to a greatly overpredicted diffusivity in the glassy state by MD simulations (and faithfully reproduced by the CRW simulations) relative to experiment [53]. Thus, in contrast to the other two applications, the prediction of the diffusivity of glassy iron is not quantitative. However, the qualitative similarity in confined diffusion remains valid. The cage size at 300 K is 0.22 Å. It is important to realize that this is the radius of a cage in which the point particle moves in the CRW simulation. A cage size for a finite-volume system would require adding the radius of the particle to this cage size. For Fe, this would correspond to a cage radius of 1.53 Å. We note that in network-forming glasses like silica, one observes a maximum in the MSD at intermediate times [54]. The simplest CRW theory as formulated in this paper is not capable of nonmonotonic behavior in the MSD as a function of observation time.

TABLE III. Properties of the MD and CRW simulations applied to the diffusion of iron at 3000 K (liquid) and 300 K (glass).

| System | $D_0$ (m$^2$/s) | $R_{\text{cage}}$ (Å) | $p_{\text{cage}}$ | $D_{\text{CRW}}$ (m$^2$/s) |
|---|---|---|---|---|
| Liquid iron | $5.9 \times 10^{-9}$ | — | 1.0 | $(5.8 \pm 0.3) \times 10^{-9}$ |
| Glassy iron | $7.6 \times 10^{-11}$ | 0.22 | $1.35 \times 10^{-4}$ | $(4.0 \pm 0.1) \times 10^{-13}$ |

## V. CONCLUSIONS

In the present work, we have developed and implemented a general theory for diffusion in the presence of nanoscale confinement. It is based on a traditional random-walk theory to which two parameters that capture confinement have been added, a cage size and cage-to-cage hopping probability. The model is extraordinarily simple; however, we have shown that it is capable of reproducing a range of behavior from completely confined to completely unconfined diffusion and it yields intermediate behavior due to confinement. The CRW theory captures the correct nonlinear dependence of the mean square displacement on observation time for intermediate times. It requires modest computational requirements and is thus able to simulate systems with very low diffusivities for a sufficiently long time to reach the infinite-time-limit regime where the MSD is linearly proportional to the observation time.

The CRW theory was applied to three systems. The application to the diffusion of RDX in IRMOF-1 demonstrated that the CRW is capable of quantitatively reproducing self-diffusivities obtained from MD simulation. Furthermore it demonstrated that the cage size parameter has a physical correspondence to the actual cage size in the IRMOF-1 material. Second, it demonstrated that temperature-dependent properties, such as the activation energy for diffusion, can also be accurately reproduced by the CRW simulations.

The application of the CRW theory to the diffusion of water in Nafion demonstrated that the CRW theory fit to short-time MSD data is capable of faithfully reproducing longer-time MSD data. This feature is useful for systems where the dynamics are sufficiently slow that reaching the Einstein limit for the diffusivity is not feasible via MD simulation alone. The CRW also generated cage size and cage-to-cage hop probabilities for water in Nafion as a function of the degree of hydration. These parameters may provide insight into the morphology of the hydrated membrane.

The application of CRW theory to the diffusion of glassy Fe demonstrated the breadth of potential applications and the ability to estimate very small diffusivities.

## ACKNOWLEDGMENTS

The authors gratefully acknowledge the financial support of the National Science Foundation (NSF) under Grant No. CMMI-0730207 and the US Department of Energy (DOE) BES under Contract No. DE-FG02-05ER15723. Work at ORNL was performed under the auspices of the Division of Materials Science and Engineering, Office of Basic Energy Science of the US Department of Energy (D.M.N.). This work used resources of the National Institute for Computational Sciences (NICS), ORNL, supported by NSF with Agreement No. OCI 07-11134.

[1] M. E. Davis, Micro. Meso. Mater. **21**, 173 (1998); E. H. Goulding, G. R. Tibbs, D. Liu, and S. A. Siegelbaum, Nature (London) **364**, 61 (1993); H. Matsuda, A. Saigusa, and H. Irisawa, *ibid.* **325**, 156 (1987); S. C. Reyes, J. H. Sinfelt, and G. J. DeMartin, J. Phys. Chem. B **104**, 5750 (2000).

[2] C. R. Martin and P. Kohli, Nat. Rev. Drug Discovery **2**, 29 (2003); C. T. Kresge, M. E. Leonowicz, W. J. Roth, J. C. Vartuli, and J. S. Beck, Nature (London) **359**, 710 (1992); J. Grumelard, A. Taubert, and W. Meier, Chem. Commun. 1462 (2004).

[3] A. I. Skoulidas, D. M. Ackerman, J. K. Johnson, and D. S. Sholl, Phys. Rev. Lett. **89**, 185901 (2002). M. Schoen, J. H. Cushman, D. J. Diestler, and C. L. Rhykerd, J. Chem. Phys. **88**, 1394 (1988); K. K. Mon and J. K. Percus, *ibid.* **117**, 2289 (2002); D. E. Moilanen, I. R. Piletic, and M. D. Fayer, J. Phys. Chem. C **111**, 8884 (2007); D. E. Moilanen, N. E. Levinger, D. B. Spry, and M. D. Fayer, J. Am. Chem. Soc. **129**, 14311 (2007); J. V. Macpherson, C. E. Jones, A. L. Barker, and P. R. Unwin, Anal. Chem. **74**, 1841 (2002); M. Kollmann, Phys. Rev. Lett. **90**, 180602 (2003); A. E. Kamholz, E. A. Schilling, and P. Yager, Biophys. J. **80**, 1967 (2001); M. Foquet, J. Korlach, W. R. Zipfel, W. W. Webb, and H. G. Craighead, Anal. Chem. **76**, 1618 (2004); G. Arora, N. J. Wagner, and S. I. Sandler, Langmuir **20**, 6268 (2004); M. P. Allen and A. J. Masters, Mol. Phys. **79**, 435 (1993).

[4] V. Kukla, J. Kornatowski, D. Demuth, I. Gimus, H. Pfeifer, L. V. C. Rees, S. Schunk, K. K. Unger, and J. Karger, Science **272**, 702 (1996).

[5] A. Einstein, Ann. Phys. (Berlin) **17**, 549 (1905).

[6] J. Crank, *The Mathematics of Diffusion* (Clarendon Press, Oxford, 1975).

[7] D. G. Levitt, Phys. Rev. A **8**, 3050 (1973).

[8] D. Keffer, H.T. Davis, and A.V. McCormick, Mol. Phys. **87**, 367 (1996).

[9] S. Kirkpatrick, Rev. Mod. Phys. **45**, 574 (1973).

[10] D. S. Sholl, Acc. Chem. Res. **39**, 403 (2006); T. Duren, Y. S. Bae, and R. Q. Snurr, Chem. Soc. Rev. **38**, 1237 (2009).

[11] D. Hofmann, L. Fritz, J. Ulbrich, C. Schepers, and M. Bohning, Macromol. Theory Simul. **9**, 293 (2000); F. Muller-Plathe, Acta Polymerica **45**, 259 (1994).

[12] M. S. Islam, J. Mater. Chem. **10**, 1027 (2000).

[13] J. W. Liu, N. Suraweera, D. J. Keffer, S. T. Cui, and S. J. Paddison, J. Phys. Chem. C **114**, 11279 (2010).

[14] F. Spitzer, *Principles of Random Walk* (Springer, New York, 1976).

[15] G. F. Lawler, *Intersections of Random Walks* (Birkhauser, Basel, 1991); D. Revuz and M. Yor, *Continuous Martingales and Brownian Motion* (Springer, Berlin, 1999).

[16] G. H. Weiss, *Aspects and Applications of the Random Walk* (North-Holland, Amsterdam, 1994).

[17] K. Falconer, *Fractal Geometry: Mathematical Foundations and Applications* (Wiley, Chichester, 1990); J. Feder, *Fractals* (Plenum, New York, 1988); J.-F. Gouyet, *Physique et Structures Fractales* (Masson, Paris, 1992); B. B. Mandelbrot and J. W. Vanness, Siam Rev. **10**, 422 (1968); B.B. Mandelbrot, *The Fractal Geometry of Nature* (Freeman, New York, 1983); H. Takayasu, *Fractals in the Physical Sciences* (Manchester University Press, Manchester, 1990).

[18] B. O'Shaughnessy and I. Procaccia, Phys. Rev. Lett. **54**, 455 (1985).

[19] H. C. Fogedby, Phys. Rev. Lett. **73**, 2517 (1994); Phys. Rev. E **50**, 1657 (1994); F. E. Peseckis, Phys. Rev. A **36**, 892 (1987); V. Seshadri and B. J. West, Proc. Natl. Acad. Sci. USA **79**, 4501 (1982); B. J. West and V. Seshadri, Physica A **113**, 203 (1982).

[20] R. Kubo, M. Toda, and N. Hashitsume, *Statistical Physics II* (Springer, Berlin, 1985), Vol. 31; R. Muralidhar, D. Ramkrishna, H. Nakanishi, and D. Jacobs, Physica A **167**, 539 (1990); K. G. Wang, L. K. Dong, X. F. Wu, F. W. Zhu, and T. Ko, *ibid.* **203**, 53 (1994); K. G. Wang and M. Tokuyama, *ibid.* **265**, 341 (1999).

[21] V. M. Kenkre, E. W. Montroll, and M. F. Shlesinger, J. Stat. Phys. **9**, 45 (1973); V. M. Kenkre, Phys. Lett. A **65**, 391 (1978); D. Bedeaux, K. Lakatos, and K. E. Shuler, J. Math. Phys. **12**, 2116 (1971); *Stochastic Processes in Chemical Physics: The Master Equation*, edited by I. Oppenheim, K. E. Shuler, and G. H. Weiss (MIT Press, Cambridge, 1977).

[22] C. Tsallis, S. V. F. Levy, A. M. C. Souza, and R. Maynard, Phys. Rev. Lett. **75**, 3589 (1995); C. Tsallis and D. J. Bukman, Phys. Rev. E **54**, R2197 (1996); L. Borland, *ibid.* **57**, 6634 (1998); A. Compte and D. Jou, J. Phys. A: Math. Gen. **29**, 4321 (1996); D. H. Zanette and P. A. Alemany, Phys. Rev. Lett. **75**, 366 (1995).

[23] R. Metzler and J. Klafter, Phys. Rep. **339**, 1 (2000).

[24] E. W. Montroll and M. F. Shlesinger, in *Nonequilibrium Phenomena II: From Stochastics to Hydrodynamics*, edited by J. L. Lebowitz and E. W. Montroll (North-Holland, Amsterdam, 1984), p. 1.

[25] G. Grimmett and D. Stirzaker, *Probability and Random Process* (Oxford University Press, Oxford, 2001).

[26] J. Rudnick and G. Gaspari, *Elements of the Random Walk: An Introduction for Advanced Students and Researchers* (Cambridge University Press, Cambridge, 2004).

[27] D. Keffer, P. Adhangale, and B. J. Edwards, J. Non-Newtonian Fluid Mech. **120**, 41 (2004).

[28] D. J. Keffer [https://trace.lib.utk.edu/home/davidkeffer/sites/atoms/animmn.html].

[29] M. Eddaoudi, J. Kim, N. Rosi, D. Vodak, J. Wachter, M. O'Keeffe, and O. M. Yaghi, Science **295**, 469 (2002).

[30] R. Xiong, J. T. Fern, D. J. Keffer, M. Fuentes-Cabrera, and D. M. Nicholson, Mol. Simul. **35**, 910 (2009).

[31] R. Xiong, D. J. Keffer, M. Fuentes-Cabrera, D. M. Nicholson, A. Michalkova, T. Petrova, J. Leszczynski, K. Odbadrakh, B. L. Doss, and J. P. Lewis, Langmuir **26**, 5942 (2010).

[32] R. Xiong, K. Odbadrakh, A. Michalkova, J.P. Luna, T. Petrova, D. J. Keffer, D. M. Nicholson, M. Fuentes-Cabrera, J. P. Lewis, and J. Leszczynski, Sens. Actuat. B Chem. **148**, 459 (2010).

[33] E. P. Wallis and D. L. Thompson, J. Chem. Phys. **99**, 2661 (1993); S. Boyd, M. Gravelle, and P. Politzer, *ibid.* **124**, 014508 (2006).

[34] S. Keskin, J. Liu, R. B. Rankin, J. K. Johnson, and D. S. Sholl, Ind. Eng. Chem. Res. **48**, 2355 (2009).

[35] P. O. Lowdin, J. Chem. Phys. **18**, 365 (1950).

[36] M. Tafipolsky, S. Amirjalayer, and R. Schmid, J. Comput. Chem. **28**, 1169 (2007).

[37] N. L. Allinger, X. F. Zhou, and J. Bergsma, THEOCHEM **118**, 69 (1994); N. L. Allinger, Y. H. Yuh, and J. H. Lii, J. Am. Chem. Soc. **111**, 8551 (1989).

[38] M. Tuckerman, B. J. Berne, and G. J. Martyna, J. Chem. Phys. **97**, 1990 (1992).

[39] S. Nosé, Mol. Phys. **52**, 255 (1984); W. G. Hoover, Phys. Rev. A **31**, 1695 (1985).

[40] S. T. Cui, J. W. Liu, M. E. Selvan, S. J. Paddison, D. J. Keffer, and B. J. Edwards, J. Phys. Chem. B **112**, 13273 (2008); S. T. Cui, J. W. Liu, M. E. Selvan, D. J. Keffer, B. J. Edwards, and W. V. Steele, *ibid.* **111**, 2208 (2007).

[41] A. Vishnyakov and A. V. Neimark, J. Phys. Chem. B **105**, 9586 (2001); **105**, 7830 (2001) D. Rivin, G. Meermeier, N. S. Schneider, A. Vishnyakov, and A. V. Neimark, *ibid.* **108**, 8900 (2004); H. C. Li, C. McCabe, S. T. Cui, P. T. Cummings, and H. D. Cochran, Mol. Phys. **101**, 2157 (2003); S. P. Gejji, K. Hermansson, and J. Lindgren, J. Phys. Chem. **97**, 6986 (1993); J. A. Elliott, S. Hanna, A. M. S. Elliott, and G. E. Cooley, Phys. Chem. Chem. Phys. **1**, 4855 (1999); S. T. Cui, J. I. Siepmann, H. D. Cochran, and P. T. Cummings, Fluid Phase Equilib. **146**, 51 (1998).

[42] W. D. Cornell, P. Cieplak, C. I. Bayly, I. R. Gould, K. M. Merz, D. M. Ferguson, D. C. Spellmeyer, T. Fox, J. W. Caldwell, and P. A. Kollman, J. Am. Chem. Soc. **117**, 5179 (1995).

[43] D. J. Price and C. L. Brooks, J. Chem. Phys. **121**, 10096 (2004); W. L. Jorgensen, J. Chandrasekhar, J. D. Madura, R. W. Impey, and M. L. Klein, *ibid.* **79**, 926 (1983).

[44] S. Urata, J. Irisawa, A. Takada, W. Shinoda, S. Tsuzuki, and M. Mikami, J. Phys. Chem. B **109**, 4269 (2005).

[45] V. A. Levashov, T. Egami, R. S. Aga, and J. R. Morris, Phys. Rev. B **78**, 064205 (2008).

[46] C. W. Gear, *Numerical Initial Value Problems in Ordinary Differential Equations* (Prentice Hall, Englewood Cliffs, NJ, 1971); ANL Report No. 7126, 1966.

[47] C. Zhu, R. H. Byrd, and J. Nocedal, ACM T. Math. Software **23**, 550 (1997); R. H. Byrd, P. H. Lu, J. Nocedal, and C. Y. Zhu, Siam J. Sci. Comput. **16**, 1190 (1995).

[48] K. D. Kreuer, Solid State Ionics **97**, 1 (1997).

[49] K. Schmidt-Rohr and Q. Chen, Nature Mater. **7**, 75 (2008).

[50] J. D. Bernal and J. Mason, Nature (London) **188**, 910 (1960).

[51] F. Faupel, W. Frank, M. P. Macht, H. Mehrer, V. Naundorf, K. Ratzke, H. R. Schober, S. K. Sharma, and H. Teichler, Rev. Mod. Phys. **75**, 237 (2003).

[52] W. Kob and H. C. Andersen, Phys. Rev. E **51**, 4626 (1995).

[53] T. Egami, JOM **62**, 70 (2010).

[54] J. Horbach, W. Kob, and K. Binder, Philos. Mag. B **77**, 297 (1998).